Sādhanā Vol. 28, Parts 1 & 2, February/April 2003, pp. 97–113. © Printed in India

Thermally assisted deformation of structural superplastics and nanostructured materials: A personal perspective

K A PADMANABHAN*

Institute of Nanotechnology, Research Center for Technology and Environment, P O Box 3640, Karlsruhe, Germany
*Present address: Sylvan International Universities, 203/204, Mahavir Chambers, Liberty Crossroads, Hyderabad 500 029, India
e-mail: kap19452002@yahoo.co.in

Abstract. Optimal structural superplasticity and the deformation of nanostructured materials in the thermally activated region are regarded as being caused by the same physical process. In this analysis, grain/interphase boundary sliding controls the rate of deformation at the level of atomistics. Boundary sliding develops to a mesoscopic level by plane interface formation involving two or more boundaries and at this stage the rate controlling step is boundary migration. In other words, grain/interphase boundary sliding is viewed as a two-scale process. The non-zero, unbalanced shear stresses present at the grain/interphase boundaries ensure that near-random grain rotation is also a non-rate controlling concomitant of this mechanism. Expressions have been derived for the free energy of activation for the atomic scale rate controlling process, the threshold stress that should be crossed for the commencement of mesoscopic boundary sliding, the inverse Hall–Petch effect and the steady state rate equation connecting the strain rate to the independent variables of stress, temperature and grain size. Beyond the point of inflection in the log stress–log strain rate plot, climb controlled multiple dislocation motion within the grains becomes increasingly important and at sufficiently high stresses becomes rate controlling. The predictions have been validated experimentally.

Keywords. Structural superplastics; nanostructured materials; grain/interphase boundary sliding.

1. Introduction

'Structural' or 'micro-grained' superplasticity in metallic materials was first reported in the early years of the twentieth century (Padmanabhan & Davies 1980; Kaibyshev 1992; Nieh *et al* 1997). Since then it has been demonstrated to be a universal phenomenon in materials having a near-equiaxed grain size of 1–20 μm (or less) that is relatively stable at the temperatures of superplastic deformation. Both already known and specially developed (pseudo-) single phase as well as microduplex metals and alloys, intermetallics, ceramics, metal/ceramic and ceramic/metal composites have all been rendered superplastic.

Mechanical behaviour of nanostructured (n-) materials has been the subject of intense research for nearly two decades (Hahn & Padmanabhan 1995a, 1995b; Padmanabhan & Hahn 1996; Morris 1998). In this paper, the mechanical properties of structural superplastics and nanostructured materials are compared. A case is made that a grain boundary sliding controlled flow model originally proposed for microcrystalline superplastic alloys (Padmanabhan & Schlipf 1996; Astanin *et al* 1996; Venkatesh *et al* 1996; Enikeev *et al* 1999) is also useful for understanding the mechanical response of nanostructured materials in the range where their behaviour resembles that of conventional materials deforming at high homologous temperatures.

Prior to developing this viewpoint, the mechanical response of n-materials is classified into two types: (a) behaviour similar to that of low homologous temperature deformation in conventional materials, and (b) that analogous to high homologous temperature deformation in materials of grain size in the micrometre range.

The low/ambient temperature behaviour as well as the post- (superplastic) forming response of structural superplastics are well documented (Padmanabhan & Davies 1980; Kaibyshev 1992; Nieh *et al* 1997). The low homologous temperature deformation behaviour of conventional materials is described in many textbooks on mechanical metallurgy.

2. Mechanical behaviour of nanostructured materials similar to the low homologous temperature deformation of conventional materials/structural superplastics

The definition that a nanostructured material has a dimension less than 100 nm at least in one direction is used. Many methods are available for the production and processing of nanocrystalline powders (see, e.g., Hahn & Padmanabhan 1995a, Padmanabhan & Hahn 1996, Morris 1998). Deagglomeration, extent of mixing, type and magnitude of pressure application (if present), nature and fineness of particles, segregation of elements to grain boundaries and new phases/compounds formed during processing all influence the mechanical properties. Therefore, the processing route/process sequence has a strong effect on the final properties. Often, many variables are left uncontrolled during processing and so at times even the reproduction of results is difficult. A review of these aspects is not attempted here.

Nanostructured materials can be produced in zero (e.g. nanoclusters), one (e.g. nanowires) or two (e.g. multi-layers) dimensions. These are not discussed in this paper. Only properties/differences in properties observed in three dimensional nanostructured materials (compared with micro-grained/conventional variants) are considered.

The following observations are consistent with what is known concerning the low homologous temperature deformation of materials of grain size in the micrometre range. They are also in agreement (where applicable) with what has been reported in literature on the post-forming properties of structural superplastics.

(i) The strength/hardness of a compact increases approximately linearly with its density. Annealing of a compact after consolidation (which decreases the flaw size and/or increases the density) or polishing of the specimen surface (which removes some flaws or reduces the size of some flaws) increases the strength and ductility.

(ii) In some cases, the enhanced mechanical properties (in n-composites) left the physical properties, e.g., magnetic properties, unchanged. In some others, e.g. n-Al5083 alloy, WC–Co Composite, the improved strength had no adverse effect on toughness/elongation at fracture.

(The increase in toughness and the decrease in the brittle to ductile transition temperature with decreasing grain size that have been demonstrated in materials of grain size in the micrometre range are yet to be established in n-materials.)

(iii) A decrease in grain size into the nm range from the mm range lowers the sintering/HIPing temperature and the sintering time. It also improves machinability after compaction.

(iv) In some systems of nm grain sizes, a direct relationship between the Young's modulus and hardness has been established.

(v) It has been concluded that grain size and shape, their distributions, pores and their distribution, other flaws/defects and their distribution, nature of the chemical bonding present in the material, impurity level, second phases/dopants, microstructures on a variety of length scales, internal stresses, surface condition, externally applied stresses and the duration of stress application and the temperature of deformation all affect the mechanical properties of n-materials. (However, no detailed studies to identify the effects of each of these variables are available.)

(vi) High cycle fatigue behaviour of bulk n–Ni samples (grain size = 50–100 nm) produced by electrodeposition was similar to that of its coarser grained counterpart. Intense shear bands, protrusions and possibly intrusions form and lead to crack formation.

(vii) In metals and intermetallics hardness increases in comparison with that of coarse grained materials, by up to a factor of 5, as the grain size is reduced into the nm range. Although qualitatively this agrees with the Hall–Petch relationship, in some cases, e.g., n–Cu, the yield stress was more than that warranted by the extrapolation based on the Hall–Petch equation. In many cases, strain hardening was absent during the room temperature deformation of nanostructured materials. This is one of the reasons (the other is poor consolidation) why the ductility of some nanostructured materials is less than that of their micrometre grained variants.

(viii) Many ceramics were brittle at room temperature. The hardness of n-ceramics and n-ceramic composites remained unchanged up to those temperatures at which diffusion and grain boundary deformation processes become important. (These temperatures, however, were lower for the nanostructured materials than for their coarser grained variants.)

(ix) In n-composites produced by annealing rapidly solidified Al and Fe based alloys, the composites were much stronger and less ductile than the fully amorphous alloy. At room temperature, these composites displayed large elastic deformation, serrated plastic flow and no work hardening. The hardness, yield strength, fracture stress and wear resistance increased with increasing volume fraction of n-particles. Their absolute values were exceptionally high compared with those of alloys of similar composition but of conventional grain size. In devitrified sputtered $Ni_{63}Ta_{23}C_{14}$ films, segregation stabilized the microduplex structure and conferred thermal stability. In the grain size range of 5–18 nm, a high hardness independent grain size was obtained, i.e., the Hall–Petch relationship was not verified. (This is not typical of high temperature behaviour either, where a direct dependence between hardness and grain size is seen.) Although the volume fraction of carbides was less, the hardness was comparable to that of cemented carbides.

(x) In n–Ni in the grain size range of 19–266 nm, the Hall–Petch relationship was obeyed. But dislocations could be seen only when the grain size was greater than about 100 nm. In some studies it has been revealed that the slope of the Hall–Petch plots decreased as the grain size went below a micrometre and remained independent of grain size over a limited grain size range below this value (Hahn & Padmanabhan 1995a).

(xi) In fully dense samples, Young's Modulus (E) was nearly equal in both the conventional and the nanocrystalline variants of a given material. (However, in porous materials, depending on the porosity level, E was lower by a factor of 2–6.)

The level of understanding with respect to this type of mechanical response of n-materials is somewhat similar to that for materials of conventional/micrometre grain sizes. It will be useful to look into the following aspects/problems in the near future: (a) why the Hall–Petch relationship does not extrapolate well when the grain size is reduced to below about a micrometre and why in some materials the hardness/flow stress is more than what is predicted by this relationship when the grain size goes into the nm range; (b) does the improvement in toughness and the lowering of the brittle to ductile transition temperature with decreasing grain size seen in materials of micrometre grain sizes persist into the nm grain size ranges and whether there is a lower limiting grain size in this regard.

3. Mechanical response of nanocrystalline materials resembling the high homologous temperature deformation of materials of conventional/micrometre range grain sizes

(i) In fully dense n–Cu, n–SnO_2 and n–TiO_2 strain rate sensitivity was present at room temperature. A nanostructured intermetallic $Fe_{28}Al_2Cr$, which was 10 times stronger than its coarse grained (75 μm) counterpart, could be subjected at room temperature to a compressive strain of 1·4.

(ii) The hardness of nanostructured materials decreased with increasing temperature of deformation, T. This has been attributed to creep.

(iii) In n–Pd and n–Cu, logarithmic creep was observed at room temperature.

(iv) In porous regions indentation, e.g., as made in a microhardness test on a nanocrystalline compact, led to local densification.

(v) In n–TiO_2 and n–ZnO, the strain rate sensitivity index, m, increased with decreasing grain size.

(vi) In n–Cu of grain size 28 nm, fracture strain increased from 15% to 55% as the strain rate was raised from 6×10^{-5} s^{-1} to $1{\cdot}8 \times 10^{3}$ s^{-1}. (This behaviour is analogous to what is seen in regions I/IIa of superplastic flow.)

(vii) In n–Ni of 30 nm grain size, significant creep that was sensitive to both temperature and strain rate could be observed at room temperature (290 K). Steady state creep was present if the applied stress was great than 600 MPa.

(viii) The strain rate sensitivity index, m, at room temperature of n–Cu was 0·036 while that of its coarse grained counterpart was 0·011. This ensured that at strain rates greater than 10^{-2} s^{-1} the *fracture stress* of n–Cu was more than that of coarse grained copper even though the *flow stress* of the former was much less, i.e., strain rate hardening was present (as during high temperature/superplastic deformation). As a result, ductility and toughness at high strain rates were superior for the nanostructured variants.

(ix) Creep behaviour, similar to what is seen in conventional ceramics, has been reported in n-ceramic powder compacts. (However, in n-ceramics creep processes and microstructural evolution commence at a lower temperature than in ceramics of conventional grain sizes.)

(x) In constant load compression tests, the strain rate of deformation decreased to zero with densification and/or grain growth. (This is the stage at which the applied stress equals the threshold stress needed for the onset of flow for the given material condition.) As in high

temperature deformation, further flow was possible only when the stress was raised to a higher value.

(xi) A compressive strain of 0·6 could be imparted to a n–TiO_2 compact of near full density at a temperature of about 0·5 Tm. The stress exponent ($N = 1/m$), was 2·2.–3·0. A nanocomposite n–TiO_2/Y_2O_3 of similar density tested at the same temperature had a value of 5·0 for N. In both materials, N was a function of density. The results could be analysed using the power law $\sigma = k\dot{\varepsilon}^m$, an equation commonly found in the literature on high temperature creep/superplasticity. (σ is the applied tensile stress, $\dot{\varepsilon}$ is the strain rate and k is a material constant.)

(xii) It has been suggested that the self and the solute diffusivities are enhanced and the thermodynamic behaviour of the grain boundary phases is different in nanostructured materials compared with materials of conventional grain sizes. (However, in some publications the diffusion behaviour of a fully dense nanocrystalline material is stated to be similar to that of materials of conventional grain sizes.)

(xiii) In many nanostructured materials, hardness/flow stress increased with increasing grain size and this is referred to as 'inverse Hall–Petch effect'. Much discussion has centred on this phenomenon. The following observations are in order (Hahn & Padmanabhan 1995; Padmanabhan & Hahn 1996; Padmanabhan 2001).

(a) When a material is very porous, hardness variation with time would be sudden. Observations concerning such specimens should be rejected.
(b) In some cases, failure arising from flaws introduced during processing could give rise to the inverse Hall–Petch effect.
(c) If an increase in grain size is achieved through annealing or raising the consolidation temperature, the flaw size and the internal stresses could have decreased and/or the density increased, along with the grain size increase. Then, it is necessary to consider the combined effects of all these changes.
(d) Morris (1998), who has taken a rather dim view of most of the experimental evidence in favour of the inverse Hall–Petch effect, has noted that this effect seen in n–Ni prepared by electrodeposition (grain size range 6–40 nm) appears to be genuine.
(e) Grain boundary processes are reported to be important during the room temperature deformation of n–Cu, n–TiAl and n–Fe_3Al/TiB_2. The flow stress of n–Cu at room temperature was much less than that of the coarse grained variety.
(f) In n–TiAl of relative density of 96% when the grain size was less than 30 nm, the inverse Hall–Petch effect was seen at room temperature and -30°C. In these experiments a change in density or evidence for dislocation activity could not be found.
(g) In dense SnO_2 inverse Hall–Petch effect was seen at room temperature.
(h) There is a case for the view that in some materials the slope of ambient/sub-ambient temperature plots of hardness, H, against the inverse square root of grain size, d (H vs. $d^{-0\cdot5}$) starts to decrease when the grain size is reduced to about one micrometre. Over a limited grain size range below this value, H is nearly independent of d. Finally, when the grain size reaches the lower ranges of the nanometre scale, the slope becomes negative.
(i) The existence of the inverse Hall–Petch effect need not be doubted. For example, during high temperature creep and superplasticity the flow stress/hardness increases with increasing grain size. In these phenomena, the onset temperature decreases with decreasing grain size. It is conceivable that for some systems this onset temperature is close to the ambient when the grain size is in the lower range of the nm scale.

(j) In ceramics, metal/ceramic and ceramic/metal composites grain boundary deformation processes like grain boundary sliding and diffusion are expected to become important only at elevated temperatures. Therefore, in these systems the inverse Hall–Petch effect is expected only at high temperatures. It is then understandable that in Fe-TiN and Ni-TiN composites hardness variation as a function of time and temperature has been seen only at elevated temperatures.

(xiv) In *in situ* studies on sputter deposited gold specimens of grain size 10 nm, intergranular crack formation and its propagation by pore formation and linkage were seen. Strain rate dependent grain boundary activity, diffusion and grain boundary sliding had a strong influence on the final ductility and toughness. (Similar observations have been made during the high temperature deformation of materials of conventional grain sizes.)

(xv) In n-composites prepared by annealing a fully amorphous alloy (obtained by rapid solidification) Newtonian viscous flow ($m = 1$) has been reported at temperatures close to the glass transition temperature and strain rate below a certain value. At higher strain rates, m, was equal to 0·25 (as in regions I and III of superplastic flow).

(xvi) Superplasticity in tension has not been reported in any nanostructured material prepared by the powder metallurgical route. But Betz *et al* (2001) could obtain 70% elongation at $0{\cdot}46T_m$ in ZrO_2–5 mol% Y_2O_3 (grain size 50 +5 nm). (This is similar to the 60% elongation Nieh *et al* (1997) obtained in ZrO_2–3 mol% Y_2O_3 of grain size 300 nm at a test temperature equal to $0{\cdot}49T_m$.) But the final grain size in the experiments of Betz *et al* (2001) was 128 nm (after 70% elongation). (Therefore, it is likely that the final grain size will be greater than 100 nm even if superplastic elongations are obtained in n-materials prepared by the powder metallurgical route.)

In contrast, in a Ti-alloy of initial grain size 20 nm prepared by severe plastic deformation, 600% elongation could be obtained at 500°C. (In the same alloy of conventional grain sizes, superplasticity could be seen only at 900–950°C.)

Some of the above observations are detailed, while the others are not. An attempt is made here to account for some of the quantitative results in terms of the grain boundary sliding controlled flow model (Padmanabhan & Schlipf 1996; Astanin *et al* 1996; Venkatesh *et al* 1996; Enikeev *et al* 1999).

4. Essential features of structural superplasticity

A recent book (Padmanabhan *et al* 2001) has listed 6 monographs, 9 reviews and 13 major conference proceedings dealing with the phenomenology, physical basis and industrial applications of structural superplasticity. A description of the different approaches to structural superplasticity and a rigorous analysis of the various constitutive equations can be found elsewhere (Padmanabhan & Davies 1980; Kaibyshev 1992; Nieh *et al* 1997; Padmanabhan *et al* 2001). In this paper, only a summary of the important experimental results that a viable theory of structural superplasticity should take into account and the explanation for this phenomenon offered by this author and his co-workers will be presented.

The mechanism described here is valid in the region of *optimal* superplastic flow, i.e., the region from the slowest strain rate to the point of inflection in the sigmoidal log stress–log strain rate isostructural, isothermal plot. Recently, it has been suggested that the range of validity of this model in some systems may extend well beyond the point of inflection

(Padmanabhan & Daniel 2001). This requires a detailed examination in a future publication. Here the treatment is restricted to the optimal range of superplastic flow, as defined above. In this region, the following important features are present.

(i) If significant grain growth is absent, the sigmoidal log stress–log strain rate curve gets shifted to lower stress levels and higher strain rates with increasing temperature and/or decreasing grain size. Temperature dependence of strain rate is exponential. The strain rate and grain size are inversely related, but in a non-linear manner.

(ii) Notwithstanding the many discussions on the relative contributions of diffusion, dislocation motion and grain boundary sliding to optimal superplastic flow, by the 1990s it was realized that nearly 100% of the external strain resulted from grain boundary sliding. The contributions from dislocation motion, in contract, fluctuated with time in such a manner that the net contribution to external strain was nearly zero (see, e.g., Valiev & Langdon 1993). However, there is evidence for limited amounts of diffusion and dislocation activity during optimal superplastic flow. Thus, a viable physical picture would be that grain/interphase boundary sliding causes the external strain, while diffusion and dislocation motion are essential for the continual operation of the sliding process in a polycrystalline material.

(iii) Transmission electron microscopy (TEM) cannot help to decide if the observed dislocation motion is rate controlling or not. In contrast, a quantitative assessment of the texture changes accompanying superplastic flow, as obtained from three dimensional ghost corrected orientation distribution function (ODF) analysis, can help in this regard because these changes represent the entire thermo-mechanical history of a material (Padmanabhan & Luecke 1986). Following a detailed experimental investigation of the texture changes accompanying superplastic flow in an Al–6Cu–0·4Zr (SUPRAL) alloy (Engler *et al* 2000), the following conclusions could be drawn (figure 1).

(a) Time at temperature had a negligible effect on the initial texture.
(b) When the alloy was deformed at room temperature $\{001\}\langle 110\rangle$ texture peak orientation changed towards orientation $\{011\}\langle 111\rangle$. This indicates dislocation slip on crystallographic planes in accordance with the predictions of Taylor poly-slip model for uniaxial stressing.
(c) Following superplastic deformation (from the onset of steady state up to a true strain $\cong 2{\cdot}0$ or percentage elongation $\cong 660\%$) at 730 K, the position of texture peaks did not change but the texture intensity decreased substantially. These results suggest that the texture was annihilated mainly by near-random grain rotations accompanying grain boundary sliding which was the rate controlling deformation mode. (The quantitative changes in texture could be analysed as a random walk problem.) Such significant grain rotations can be present only when the grain boundary shear stresses are non-zero and are unbalanced. They will not be present if grain boundary sliding is a rapid accommodation process and the grain boundary shear stresses instantaneously relax to zero, as assumed, e.g., in the Ashby & Verrall (1973) model. Intergranular dislocation slip control, on the other hand, will lead to totally different texture changes.

5. A model for optimal structural superplasticity and temperature-sensitive deformation of nanostructured materials

This model (Padmanabhan *et al* 1995; Padmanabhan & Schlipf 1996; Astanin *et al* 1996; Hahn & Padmanabhan 1997; Venkatesh *et al* 1996; Enikeev *et al* 1999) applies to steady state struc-

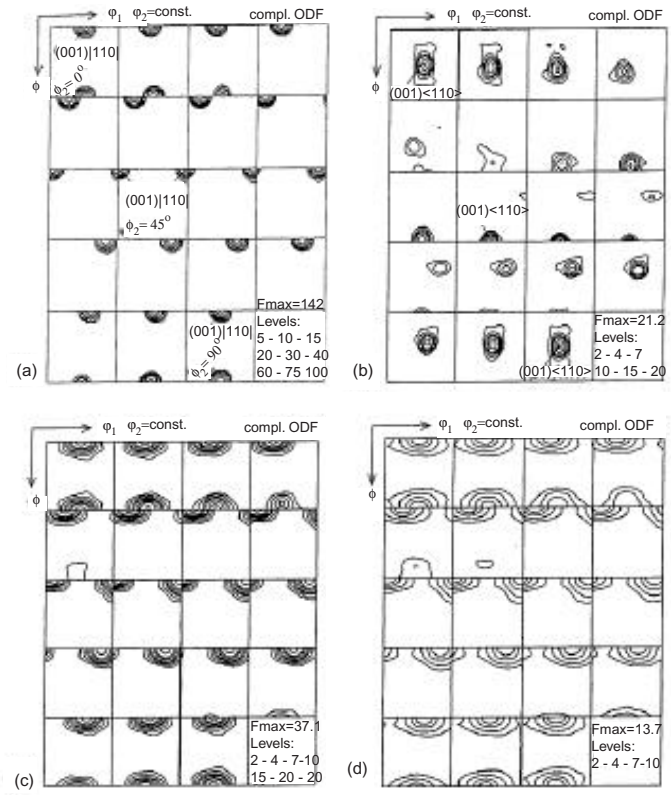

Figure 1. Texture at different states of deformation: **(a)** undeformed state (grip section, soaked at 730 K); **(b)** deformed by 92% at room temperature; **(c)** deformed by 175% ($\varepsilon \sim 1$) at 730 K; and **(d)** deformed by 660% ($\varepsilon \sim 2$) at 730 K.

tural superplasticity and may also be used to understand the deformation of nanostructured materials of the type described in § 3. It does not account for the type of results described in § 2 (which resembles low homologous temperature response in conventional materials and structural superplastics).

In this approach the rate controlling flow is confined to a network of deforming grain - and interphase-boundaries that surround essentially non-deforming grains except for what is required to achieve strain and geometric compatibility (figure 2). Boundaries of high viscosity can be bypassed by grain rotation (Engler *et al* 2000).

According to Wolf (1990) a high angle boundary contains excess free volume of the order of 0·10 Ω, where Ω is the atomic volume in the lattice. This free volume is not distributed continuously along the boundary but is concentrated at certain sites that depend on the orientation and misfit of the boundary. An atomic ensemble around a free volume site is regarded as the basic unit of sliding. A high angle boundary comprises many such basic units. For mathematic treatment, the basic unit has been assumed to be an oblate spheroid of ground area πw^2 in the grain boundary plane and radius on either side of the boundary of $(w/2)$, where w is the grain boundary width. Thus, the volume of a basic unit $V_o = \pi w^3$. It is assumed that the basic units of flow can undergo shear transformations independent of each other.

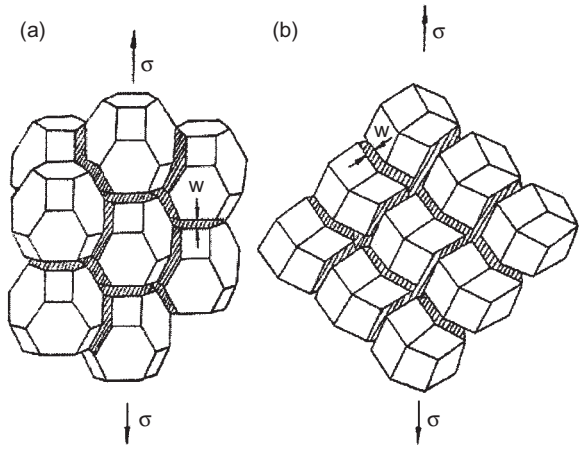

Figure 2. Schematic showing the regions of rate controlling flow (shaded) in a polycrystalline material with grains of idealized shapes. **(a)** Tetrakaidecahedral; **(b)** rhombic dodecahedral.

Due to the presence of free volume, around a free volume site there would be many metastable configurations whose free energies would differ only by a small amount. The initial atomic configuration in the ensemble would correspond to the lowest free energy. At a high homologous temperature, most of the energy of activation would be available from thermal energy. Then, the basic unit can shear to a neighbouring configuration if the shear stress exceeds $\tau(= \Delta F_i/\gamma_i V_o)$ where ΔF_i is the free energy of the shear transformation (equal to the difference between the free energy of the new configuration and that of the original one) and γ_i is the strain associated with a unit shear event. That is, for stresses $\tau \geq \tau_i$ the neighbouring configuration C is topologically equivalent to C'_{eq} and forms the new equilibrium configuration C'_{eq}. Again there will be metastable states C'' nearby, which can be transformed by the action of τ_i to a lower energy state of C''_{eq} equal to C_{eq}. Thus grain boundary sliding can proceed by a sequence of shear transformations. The equivalence of C_{eq} and C'_{eq} constitutes iso-configurational flow kinetics which can be described by transition state theory (Padmanabhan & Schlipf 1996).

Another result of the analysis of Wolf (1990) is that the excess free volume at a high angle boundary varies only slightly with misorientation. Therefore, the individual shear transformation γ_i and the accompanying transient volume expansion ε_i as the basic unit embedded in a solid matrix shears into a new position will not differ much for the different basic units or for the different metastable states within a basic unit. Therefore, γ_i and ε_i can be replaced by their averages γ_o and ε_o respectively.

According to Eshelby (1957), the elastic energy due to a shear γ_o in the basic unit is given by

$$\Delta F_1 = 1/2\beta_1 G V_o \gamma_o^2, \tag{1}$$

where G is the shear modulus. The elastic energy due to concomitant transient volume expansion ε_o is

$$\Delta F_2 = 1/2\beta_2 G V_o \varepsilon_o^2. \tag{2}$$

For an oblate spheroid, $\beta_1 = 0{\cdot}944(1{\cdot}590 - p)/(1 - p)$ and $\beta_2 = 4(1 + p)/[9(1 - p)]$, with p the Poisson ratio (Eshelby 1957). It is suggested that the sum of the elastic energies

of the shear and the transient volumetric distortions constitutes the free energy of activation $\Delta F_0 (= \Delta F_1 + \Delta F_2)$ for the boundary sliding process at a grain boundary.

In high temperature creep, steric hindrance makes this atomic scale sliding rather ineffective and causes triple point cracking and premature failure. In order to produce substantial sliding on a mesoscopic scale (defined to be of the order of a grain diameter or more) two or more boundaries must cooperate to form a plane interface which by interconnection with other similar plane interfaces can lead to long range sliding until stopped by an insurmountable barrier, e.g., an extra large grain or a coarse precipitate. The driving force for plane interface formation is the reduction in the overall grain boundary energy through a reduction in the grain boundary area in the direction of sliding and this is achieved through grain boundary migration (Padmanabhan & Schlipf 1996; Astanin *et al* 1996a) (figure 3). (Very recently it has been concluded that the driving force for this process in the general case is the minimization of the Gibbs free energy of the system and this will be reported elsewhere.) In the early stages, deformation would be predominantly along those boundaries at which the critically resolved shear stress is the largest and these boundaries would stand out in relief. At large strains, all boundaries would have deformed nearly equaly and so the plane interfaces will have to be carefully identified in a metallographic examination.

Thus, in this approach grain/interphase boundary sliding is visualized as a two scale phenomenon. On the microscopic scale, the obstacles to sliding are localized and can be overcome by thermal activation. Short range internal stresses develop at this level. On a mesoscopic scale, the obstacles to sliding are other grains or particles residing at grain/interphase boundaries. The internal stresses associated with sliding at this level have a long range and manifest themselves as a threshold stress (which should be subtracted from the applied stress to know the effective stress driving the microscopic scale sliding process).

The physical picture for the mesoscopic boundary sliding process is as follows. The polycrystalline structure is described as a cubic dense packing of equisized spheres. Let the walls of the Wigner-Seitz cell containing one sphere represent the grain boundaries. This corresponds to a face centered cubic structure on a mesoscopic scale with glide planes and glide directions. Since the roughness is the least on the mesoscopic {111} planes, these are assumed

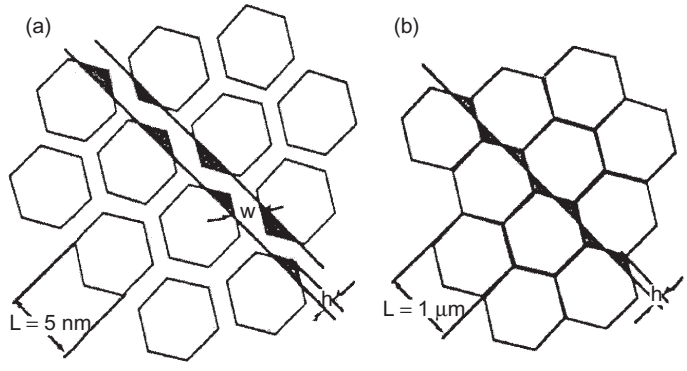

Figure 3. 2D schematic for plane interface formation in **(a)** nano ($W/L = 01, L = 5\,\text{nm}$) and **(b)** micrometre ($W/L = 0005, L = 1\,\mu\text{m}$) grained materials Atoms in the darker regions have to be rearranged by local boundary migration.

to be the glide planes for long range sliding. The surface of the {111} plane in the mesoscopic structure consists of a regular arrangement of peaks and troughs whose height 'h' will vary as the average grain size L regardless of grain shape. Likewise, the ground area A will vary regardless of grain shape as L^2 (figure 3).

In order to create a plane interface, the peaks and troughs of the mesoscopic {111} plane must be removed, i.e., the grain boundary area along the mesoscopic glide plane must be decreased by local migration.

Local boundary migration can take place in two ways (Perevezentsev *et al* 1992; Padmanabhan & Schlipf 1996).

(a) It can take place entirely by diffusion. The number of grain boundaries that align to form the plane interface will then depend on the temperature of deformation and grain size as the extent of diffusion possible will depend on temperature and the grain size determines the height of peaks and the depth of troughs to be filled by diffusion. Evidently, due to energy considerations, the number of grain boundaries that form the plane interface will also depend on the magnitude of the specific grain boundary energy, γ_B.

(b) It can take place by a combination of dislocation emission and diffusion. Initially sliding gets blocked at a peak in the boundary array on the mesoscopic {111} plane. This will give rise to a stress concentration. With more and more slid regions pushing against the peak , (i) the misfit increases, and (ii) the magnitude of the stress build up increases. When the misfit and the stress developed equal the values needed for emitting a lattice dislocation from the grain boundary into the grain of the given orientation, this will happen either during a thermal event or in a barrier free manner (Perevezentsev *et al* 1992). As the total misfit to be eliminated from the boundary will/need not be an exact multiple of the Burgers vector of the lattice dislocation for the given boundary misorientation, the residual misfit (which will be a function of the Burgers vector) will have to be removed by diffusion.

When two phases differ significantly in composition at an interface formed by them the mechanism described in (b) is likely to operate (as diffusion distances of the order of grain size would be involved, if boundary migration were to take place entirely by diffusion). At an intercrystalline boundary as the mechanisms described in both (a) and (b) can operate, the one that is energetically more favourable will be preferred. With this physical picture, it is possible to calculate the threshold stress needed for plane interface formation via the two mechanisms described in (a) and (b) above.

As the peaks and troughs get filled during plane interface formation, the grain boundary area perpendicular to this plane will increase (figure 4). Let this increase in area per grain be ΔA and the number of boundaries participating in a mesoscopic sliding event be N. For further calculations, the grain size is taken to be of a uniform value L and the grain shape is considered to be rhombic dodecahedron.

In the lower grain size ranges of nanostructured materials the peak height becomes comparable to the grain boundary width, W, and eventually for an ultrafine grain size L_o, h will be equal to W. Then, sliding can spread from one boundary to the next without the need to overcome a threshold stress, i.e., for a grain size $L = L_o$, the threshold stress is zero.

Quantitative development of the above ideas leads to the following expression for the threshold stress for plane interface formation in the shear mode, τ_o.

$$\tau_0 = \left[2G\gamma_B(\Delta A/A)/\alpha_f(NA)^{0{\cdot}5}\right]^{0{\cdot}5}, \tag{3}$$

where $\alpha_f =$ a form factor of the order of unity.

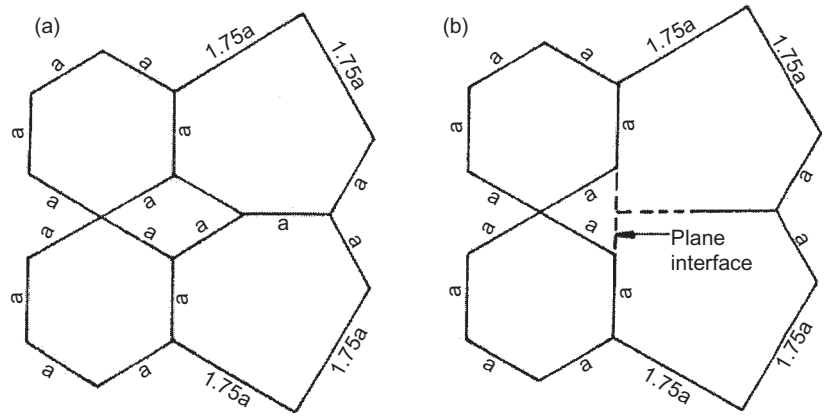

Figure 4. Schematic to show that plane interface formation decreases boundary area in the direction of sliding but increases grain boundary area perpendicular to that direction. **(a)** Prior to and **(b)** after deformation.

For rhombic dodecahedron grain shape,

$$h = (6^{0{\cdot}5}/12)L,\ A = (3^{0{\cdot}5}/4)L^2 \text{ and } \Delta A = (2^{0{\cdot}5}/8)\left[L^2\left(1 - (2x6^{0{\cdot}5}W/L)\right)\right]. \tag{4}$$

It is easy to see that for this case the shear resistance to plane interface formation will vanish when $L = L_0 = 2 \times 6^{0{\cdot}5}W$. Further analysis reveals that if

$$L_1 = 2^{1{\cdot}5}x3^{-0{\cdot}75}N^{-0{\cdot}5}\gamma_B/G\alpha_f, \tag{5}$$

$$\tau_o = G\left[(L_1/L)\left(1 - (L_o/L)\right)\right]^{0{\cdot}5};\ L \geq L_o, \tag{6}$$

$$\tau_o = 0;\ L < L_o, \tag{7}$$

$$\tau_o = G\left(L_1/L\right)^{0{\cdot}5};\ L \gg L_o. \tag{8}$$

In real materials, a grain size distribution will be present. Grain shape will be irregular. In two phase materials the proportion of phases and the nature of phase distribution will decide the details of the mesoscopic sliding event. For all these cases the exponent 0·5 in (6) and (8) should be replaced by a_1, with the condition that $0 < a_1 < 0{\cdot}5$. a_1 is obtained experimentally from a plot of τ_o Vs. L. Likewise, N is also determined experimentally. (Recently, it has been possible to develop the analysis of the grain boundary migration process further and it is no longer necessary to have these two experimental inputs. This will be reported elsewhere.)

Using transition state theory, the following rate equation can be obtained in the tensile mode (Padmanabhan & Schlipf 1996; Padmanabhan 2000).

$$\dot{\varepsilon} = A_1 \sinh[B[\sigma - \sigma_0]];\ \sigma \geq \sigma_0, \tag{9}$$

where, $A_1 = (5{\cdot}77b\varepsilon_0\nu/L)\exp\left(-\Delta F_0/KT\right)$, $B = 6\pi b^3\varepsilon_0/KT$, with b the nearest neighbour interatomic spacing in the grain boundary region, ν the thermal vibration frequency and K the Boltzmann constant. σ_0, the threshold stress in the tensile mode, is equal to $3^{0{\cdot}5}\tau_0$. For small stresses ($\sinh x \sim x$)

$$\dot{\varepsilon} = A'(\sigma - \sigma_0);\ A' = A_1B. \tag{10}$$

$\Delta F_0 = Q - T\Delta S$, where Q is the activation energy for the sliding process and ΔS is the entropy of activation for this process. It is also possible to develop (9) with an additional assumption to a quadratic form for the strain rate as a function of the applied stress (Padmanabhan & Schlipf 1996; Enikeev *et al* 1999; Betz *et al* 2001).

The grain size dependence of strain rate obeys the relationship (Betz *et al* 2001)

$$\ln \dot{\varepsilon} = A_2 - \ln L - \left(A_3/L^{a_1}\right), \sigma > \sigma_0, \tag{11}$$

where A_2 and A_3 are constants and the suffix σ indicates that this variable is kept constant. Equations (1)–(11) are obeyed by both structural superplastics and n-materials at strain rates up to that corresponding to the point of inflection in the $\log\sigma$–$\log\dot{\varepsilon}$ curve.

6. Behaviour beyond the strain rate at the point of inflection

In this region climb controlled multiple dislocation motion within the grains starts to operate and becomes increasingly important as the stress level is raised. Eventually, at a sufficiently high stress, this process becomes rate limiting. An equation that can be used to describe this region is the one given by Weertman (see Padmanabhan & Daniel 2001), viz.,

$$\dot{\varepsilon}_{\text{disloc}} = \left[\alpha_1 D\Omega/(G^{3{\cdot}5}kT)\right]\sigma^{4{\cdot}5}, \tag{12}$$

where $\alpha_1 = 5 \times 10^{20}$ cm^{-2}, $n = 1/m = 4{\cdot}5$ and $D =$ bulk diffusion coefficient. This region is not likely to be found in nanostructured materials when the grain size is too small to allow the nucleation of dislocations within a grain.

7. Inverse Hall–Petch effect

In this analysis, (6)/(8) is the mathematical form of the inverse Hall–Petch effect reported in literature on nanostructured materials. As this effect is often demonstrated using a microhardness test, (6) has been expressed as (Padmanabhan *et al* 1995; Hahn & Padmanabhan 1997)

$$H = H_a - H_0, \tag{13}$$

where, H is the measured hardness, H_a is the hardness on load application and $H_0 = (\tau_0/C)$ where C is the (unknown) proportionality constant that relates hardness to yield/flow stress. Therefore,

$$H = H_a - \left(m^2/L\right)(L - L_0)^{0{\cdot}5}; m_2 = \left(GL_1^{0{\cdot}5}/C\right). \tag{14}$$

8. Hardness variation as a function of time in n-materials

It is easy to show (Padmanabhan 2000) that $\dot{H}/H\alpha\dot{\varepsilon}$, where H is the hardness and $\dot{H}$ is its time derivative . As $H\alpha\sigma$ and the equation $\dot{\varepsilon} \propto \sigma^n$ is obeyed, one can obtain

$$H = H_{\max} - (H_{\max}/n)\ln(Bt + 1), \tag{15}$$

where B is a fitting constant and $H_{\max}$ is the hardness on load application. Equation (15) describes the hardness drop as a function of time in n-materials exhibiting the type of mechanical behaviour described in § 3.

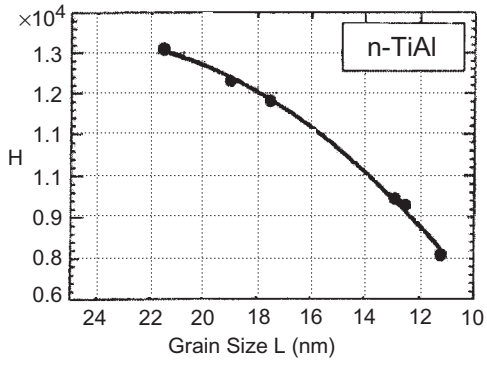

Figure 5. A least squares fit in terms of (14), room temperature microhardness-grain size data for n–TiAl. H is in megapascals The grain boundary width, W, for this material is predicted as 056 nm.

9. Experimental validation

The analysis has been validated for a number of systems involving both structural superplastics and nanostructured materials (Padmanabhan *et al* 1995; Venkatesh *et al* 1996; Hahn & Padmanabhan 1997; Enikeev *et al* 1999; Padmanabhan 2000; Betz *et al* 2001; Padmanabhan & Daniel 2001). So only very few examples are given here.

From (6)/(14) it is clear that the grain boundary width can be predicted from microhardness measurements on an n-material. Using this equation the grain boundary width has been predicted correctly in the case of n–Pd, n–$NbAl_3$, n–Cu and n–TiAl. Figure 5 pertaining to n–TiAl is an example. It has also been possible to conclude that during the room temperature deformation of n–Cu the inverse Hall–Petch effect can be observed only below a grain size of about 50 nm (Hahn & Padmanabhan 1997).

Figure 6 demonstrates that in nanostructured Fe-63 vol% TiN the hardness variation with time follows 15.

Equation (9) has been shown to be obeyed by many superplastic Al alloys and Yttria stabilized ZrO_2 (Enikeev *et al* 1999; Betz *et al* 2001). In figure 7 corresponding to the Al-13wt.%

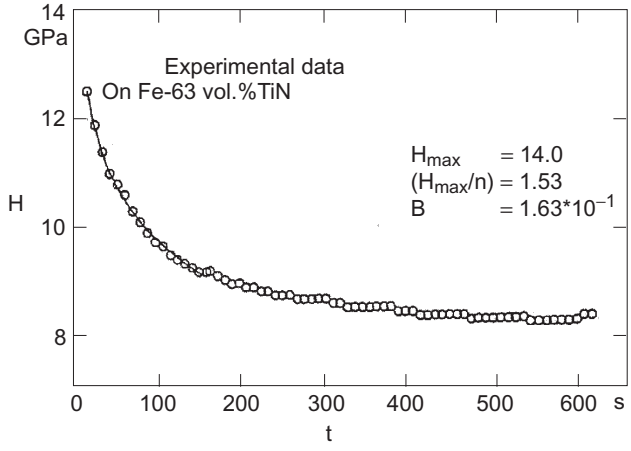

Figure 6. Hardness variation with time in Fe-63 vol% TiN which obeys (15).

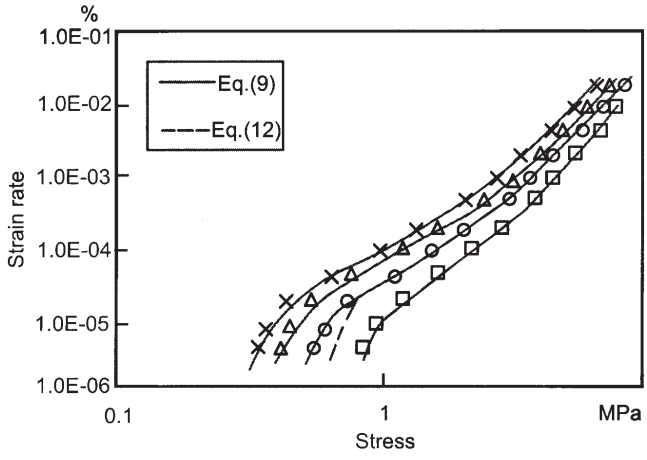

Figure 7. Sigmoidal steady state log strain rate-log stress relationship in an Al–Si eutectic alloy The symbols indicate experimental points. Full curves are according to (9). Dotted lines obey (12).

Si eutectic alloy, it is shown that (9) is valid up to the point of inflection in the $\log\sigma$–$\log\dot{\varepsilon}$ plot and (12) governs the flow beyond that point, as required by the present analysis. The grain size dependence of strain rate in case of sub-microcrystalline ZrO_2–3mol% Y_2O_3 is shown to obey (11) in figure 8. *Ab initio* calculation of the activation energy for the rate controlling flow process using (1) and (2) has also been shown to be accurate (Betz *et al* 2001).

10. Conclusions

A unified analysis for the high homologous temperature deformation of structural superplastics and nanostructured materials has been presented. In this model, grain/interphase

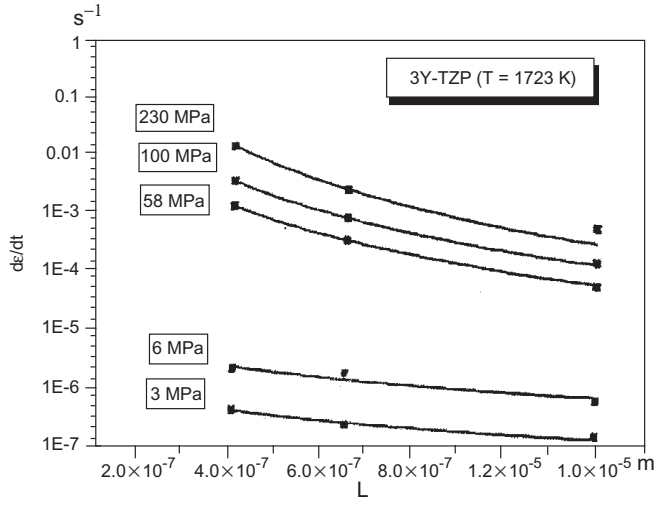

Figure 8. Log strain rate versus grain size plots according to (11) in $ZrO_2 - 3$ mol% Y_2O_3 (3Y-TZP) polycrystalline material.

boundary sliding is the rate controlling process at atomistic level. This sliding process, which is blocked at triple junctions and other grain boundary obstacles during high temperature creep, develops to a mesoscopic scale (defined to be of the order of a grain diameter or more) during high homologous temperature deformation in structural superplastics and nanostructured materials. The analytical treatment leads to expressions for the free energy of activation for the rate controlling process, the threshold stress that has to be overcome for the commencement of mesoscopic sliding, the inverse Hall–Petch effect and the steady state rate equation that connects the observed strain rate to the experimental variables of stress, temperature and grain size. It is also concluded that beyond the point of inflection in the $\log\sigma$–$\log\dot{\varepsilon}$ curve climb controlled multiple dislocation slip within the grains becomes increasingly important and eventually rate controlling. The predictions of the model have been validated using experimental results.

This paper was written during the period the author was at the Institute of Nanotechnology, Research Center, Karlsruhe, Germany. He thanks Prof.-Dr H Gleiter for constant encouragement.

References

Ashby M F, Verrall R A 1973 Diffusion-accommodated flow and superplasticity. *Acta Metall.* 21: 149–163

Astanin V V, Faizova S N, Padmanabhan K A 1996a A model for grain boundary sliding and its relevance to optimal structural superplasticity: Part 2. Evidence for cooperative grain/interphase boundary sliding and plane interface formation. *Mater. Sci. Technol.* 12: 489–494

Astanin V V, Padmanabhan K A, Bhattacharya S S 1996b A model for grain boundary sliding and its relevance to optimal structural superplasticity: Part 3. The effects of flow localization and specimen thickness on superplasticity in alloy supral 100. *Mater. Sci. Techol.* 12: 545–550

Betz U, Padmanabhan K A, Hahn H 2001 Superplasic flow in nanocrystalline and sub-microcrystalline yttria-stabilized tetragonal zirconia. *J. Mater. Sci.* 36: 5811–5821

Eshelby J D 1957 The determination of the elastic field of an ellipsoidal inclusion, and related problems. *Proc. R. Soc. London* A241: 376–396

Engler O, Padmanabhan K A, Luecke K 2000 Superplastic flow induced texture annihilation. *Modelling Simul. Mater. Sci. Eng.* 8: 477–490

Enikeev F U, Padmanabhan K A, Bhattacharya S S, 1999 Model for grain boundary sliding and its relevance to optimal structural superplasticity: Part 5. A unique numerical solution. *Mater. Sci. Technol.* 15: 673–682

Hahn H, Padmanabhan K A 1995a Mechanical response of nanostructured materials. *Nanostruct. Mater.* 6: 191–200

Hahn H, Padmanabhan K A 1995b Deformation behaviour and possible applications of nanostructured materials. *Advanced materials processing*. (Proc. Second Pacific Rim Int. Conf. on Advanced Materials Processing, PRICM-2) (Kyongju, Korea: Korean Institute of Metals and Materials) vol. 3, pp 2119–2125

Hahn H, Padmanabhan K A 1997 A model for the deformation of nanocrystalline materials. *Philos. Mag.* B76: 559–571

Kaibyshev O A 1992 *Superplasticity in alloys intermetallides and ceramics*. (Heidelberg/Berlin: Springer Verlag)

Morris D G 1998 Mechanical behaviour of nanostructured materials. *Materials Science Foundation 2* (Aedermannsdorf, Switzerland: Trans. Tech. Publ.) pp 1–86

Nieh T G, Wadsworth J, Sherby O D 1997 *Superplasticity in metals and ceramics* (Cambridge: University Press)

Padmanabhan K A 2000 Deformation of structural superplastics, nanostructured materials and metallic glasses: A unified approach. *J. Metastable Nanocryst. Mater.* 8: 753–760

Padmanabhan K A 2001 Mechanical properties of nanostructured materials. *Mater. Sci. Eng.* A304–306: 200–205

Padmanabhan K A, Daniel B S S 2001 Unified theory of deformation for structural superplastics, metallic glasses and nanocrystalline materials. *Proc. Int. Conf. Superplasticity in Advanced Materials (ISCAM 2000)* (Aedermannsdorf, Switzerland: Trans. Tech. Publ.) pp 371–380

Padmanabhan K A, Davies G J 1980 *Superplasticity* (Heidelberg/ Berlin: Springer Verlag)

Padmanabhan K A, Hahn H 1996 Microstructure, mechanical properties and possible applications. *Proc. Symp. on Synthesis and Processing of Nanocrystalline Powder* (Warrendale: Miner. Met. Mater. Soc.) pp 21–32

Padmanabhan K A, Luecke K 1986 An assessment of the role of texture in structurally superplastic flow. *Z. Metallkl.* 77: 765–770

Padmanabhan K A, Nitsche R, Hahn H 1995 On the deformation of nanocrystalline metals and ceramics. *EUROMAT 95, the 4th Int. Conf. Adv. Mater. and Processes, Symp. G: Special and Functional Materials* (Milano: Associazone Italiana Di Metallurgica) pp 289–298

Padmanabhan K A, Schlipf J 1996 A model for grain boundary sliding and its relevance to optimal structural superplasticity: Part 1. Theory. *Mater. Sci. Techol.* 12: 391–399

Padmanabhan K A, Vasin R A, Enikeev F U 2001 Superplastic flow: *Phenomenology and mechanics*. (Heidelbeg/Berlin: Springer Verlag)

Perevezentsev V N, Rybin V V, Chuvildeev V N 1992 The theory of structural superplasticity - II. Accumulation of defects on the intergranular and interphase boundaries. Accommodation of the grain boundary sliding. The upper bound of the superplastic strain rate. *Acta Metall.* 40: 895–905

Valiev R Z, Langdon T G 1993 An investigation of the role of intragranular dislocation strain in the superplastic Pb-62% Sn eutectic alloy. *Acta Metall.* 41: 949–954

Venkatesh T A, Bhattacharya S S, Padmanabhan K A, Schlipf J 1996 A model for grain boundary sliding and its relevance to optimal structural superplasticity: Part 4. Experimental verification. *Mater. Sci. Technol.* 12: 635–643

Wolf D 1990a Structure-energy correlation for grain boundaries in *fcc* metals: III. Symmetrical tilt boundaries. *Acta Metall.* 38: 781–790

Wolf D 1990b Structure-energy correlation for grain boundaries in *fcc* metals: IV. Asymmetrical twist (general) boundaries. *Acta Metall.* 38: 791–798